

REGULAR ARTICLE

# Dimeric conformation sensitive electronic excited states of tetracene congeners and their unconventional non-fluorescent behaviour

N AGGARWAL<sup>a,b</sup> and A PATNAIK<sup>a,\*</sup> 

<sup>a</sup>Colloids and Interface Chemistry Laboratory, Department of Chemistry, Indian Institute of Technology Madras, Chennai 600 036, India

<sup>b</sup>Department of Chemistry and Biochemistry, Sharda University, Greater Noida, Uttar Pradesh 201 310, India  
E-mail: archita@iitm.ac.in

MS received 27 August 2018; revised 2 April 2019; accepted 3 April 2019; published online 5 June 2019

**Abstract.** Unconventional non-fluorescent J-aggregates of Tetracene (TC) and Naphtho[2,1,8-*qra*]tetracene (NT) were witnessed and their consequent dramatic quenching was unravelled by a steady state, time-resolved and transient spectroscopy in conjunction with excited state density functional calculations. The TC O-aggregate with slippage angle  $\theta = 22.3^\circ < 54.7^\circ$  exhibited substantial transition dipole moment (TDM) for both lower (2.79 D) and higher (1.59 D) energy singlet excitations, while, NT formed an ideal J-aggregate (polarization angle,  $\alpha \sim 0^\circ$ ) with a predominant TDM to only a lower excitonic state (2.69 D). Subsequently, their unusual quenching was quantified with large drops in the photoluminescence quantum yields (PLQY) from 0.116 to 0.002 upon TC O-aggregation and from 0.478 to 0.038 upon NT J-aggregation. These intense PL drops were systematically investigated for possible occurrence of excimer-like emission quenching and/or photo-degradation of the TC core unit. In view of the TC O-aggregates exhibiting a perfect energetic balance between the singlet (2.34 eV) and triplet (1.28 eV) energies for singlet fission (SF) and a concomitant delayed fluorescence signal, their  $S_1$  decay characteristics were attributed to SF followed by an inverse triplet-triplet recombination. In contrast, the energetic imbalance ( $E(S_1) < 2x E(T_1)$ ) in NT J-aggregates permitted only forward process of SF and the resulting long-lived triplet formation was traced with a positive transient absorption ( $T_1 \rightarrow T_n$ ) band at 500 nm. Accordingly, the singlet excited state ( $S_1$ ) dynamics of TC O- and NT J-aggregates, being largely dominated by SF, depicted a depleted  $S_1$  population, accounting for the large deviation from aggregation induced enhanced emission, exhibited by classical dye J-aggregates.

**Keywords.** Non-fluorescent J-aggregates; transition dipole moment; DFT; excited state; singlet fission.

## 1. Introduction

Highly ordered molecular aggregates<sup>1,2</sup> have been classified on the basis of their slippage angle ( $\theta$ ), defined as the angle subtended by the line joining monomeric centers and the monomeric electronic transition dipole moment (TDM) (cf. Figure 1(a)).<sup>3</sup> It is well known that the strong monomeric coupling in J-aggregates ( $\theta \leq 54.7^\circ$ ) results in a coherent excitation at a pronounced red-shifted wavelength in reference to the monomer.<sup>2,3</sup> Moreover, J-aggregates following the exciton coupling model<sup>3</sup> demonstrated a manifold fluorescence enhancement leading to the dramatic improvement in

the photoluminescence quantum yield (PLQY).<sup>4-6</sup> In contrast, the rapid internal conversion of the allowed higher energy exciton state to the forbidden lower energy exciton state has quenched the fluorescence in H-aggregates ( $\theta \geq 54.7^\circ$ ).<sup>3</sup> Although existing reports on some of the emissive H-aggregates have clearly proven the violation of exciton coupling model,<sup>7-9</sup> the unusual non-emissive behavior in J-aggregates are rare.<sup>10,11</sup> However, it is worth mentioning that ever since the discovery of J-aggregates in the 1930s,<sup>12</sup> the scientific interest in their structural and photophysical properties were limited only to a certain class of dyes.

\*For correspondence

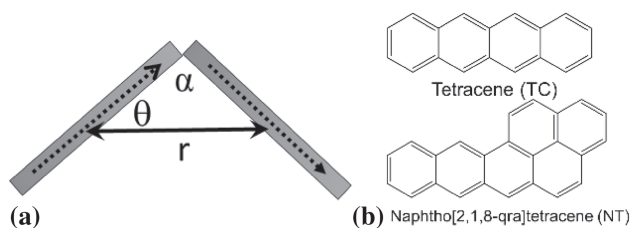


**Figure 1.** (a) Schematic diagram of a molecular dimer depicting a slippage angle,  $\theta$  (angle subtended by monomeric transition dipole moment (TDM) and molecular centres) and polarization angle,  $\alpha$  (angle subtended by monomeric TDMs). (b) Chemical structures of the TC and NT molecules. Hydrogen atoms are removed for clarity.

Polyacenes and their derivatives have been used in a plethora of applications such as solar cells,<sup>13–17</sup> light-emitting diodes<sup>18–20</sup> and organic field-effect transistors<sup>21,22</sup> to name a few. It is well-understood that in some polyacenes, the singlet excited state dynamics is largely dominated by a spin-allowed singlet fission (SF) process that involves the conversion of a singlet exciton to two nascent electron-hole pairs *via* long-lived triplet formation.<sup>23</sup> Moreover, the SF process is observed to occur at an ultrafast time scale (80 fs – 25 ps)<sup>17,23,24</sup> leading to a rapid decay of an excited singlet to the lowest triplet. Consequently, as SF takes place, the singlet excited state population within an acene could deplete. Indeed, SF was first introduced by Schneider and co-workers in 1965 to explain the fluorescence quenching in crystalline anthracene;<sup>25</sup> however, the technological development of SF-based materials has outstripped the fundamental understanding of their photoluminescence (PL) behavior. In molecular dimers, SF by direct coupling has served much better by slip stacking than by linearly linking the chromophores.

While our recently published<sup>11</sup> unusually non-fluorescent colloidal J-aggregates of Rubrene were explained *via* SF, the motivation of this study was to explore whether the documented SF can significantly affect the PL behavior in the J-aggregate nuclear conformations of structurally different (from Rubrene), but belonging to a similar class of polyacenes. Tetracene (TC) and its derivatives represented a perfect energetic balance (i.e.,  $E(S_1) \sim 2xE(T_1)$ ) for both SF as well as its inverse process of triplet-triplet recombination.<sup>26,27</sup> Consequently, the excited singlet and triplet state dynamics of TC have been largely monitored *via* prompt and delayed fluorescence (DF) signals, respectively.<sup>28–32</sup> This established nature of SF makes TC an ideal system for the investigation of SF impact on its PL behavior. However, in literature, several other factors have also accounted for explaining the complex PL

behavior. Swenberg and Stacy in 1968 have reported the anomalously low PL quantum yield (0.2%) in TC crystals which was tentatively assigned to thermally activated dissociation of singlet excitons.<sup>33</sup> Moreover, a long wavelength excimer-like emission at 600 nm was also evident in amorphous TC films.<sup>34</sup> Furthermore, previous studies have found evidence of naphthalene-like emission features in TC introduced by the oxidation of TC.<sup>35–37</sup> Bardeen *et al.*, observed a 50 ps emission in TC nanocrystalline particles, attributed to a thermal distribution of super-radiant exciton states extending over  $\sim 10$  TC molecules.<sup>38</sup> Therefore, although the excited state dynamics of TC is known to be largely dominated by an ultrafast SF process, investigation of SF consequential PL origin in TC molecular aggregates demanded a careful attention. TC although represents a prototypical molecule for the investigation of SF impact on PL, its dimeric conformation in single crystalline and polycrystalline forms was noticed to slightly deviate from an ideal J-dimer.<sup>38,39</sup> Therefore, Naphtho[2,1,8-qr]tetracene (NT) (cf. Figure 1(b)), consisting of a molecular backbone structurally equivalent to TC, was also investigated in the present work. The molecular structure of NT was thought of supporting an ideal J-aggregation promoted by enhanced  $\pi$ - $\pi$  and minimized C-H stacking interactions.

Literature cites optical absorption in J-aggregate nuclear geometry to be associated with the lowest bound exciton state with a predominant charge transfer (CT) character.<sup>1</sup> Interestingly, the role of CT states in accelerating SF was also recognized,<sup>23,40</sup> and recently a theoretical framework based on the role of CT states have predicted large effects on the SF rates by changing the chromophore - chromophore interaction geometry.<sup>41,42</sup> Along with Kasha's Coulomb-coupled ensembles, a report by Hestand and Spano<sup>43</sup> described short-range, CT mediated interactions in the varied J and H nuclear geometries. Therefore, in the present investigation, the accurate determination of CT character associated with singlet excited states of TC and NT aggregates was also established *via* electronic structure calculations.

## 2. Experimental

### 2.1 UV-Vis absorption and steady state emission characteristics

TC and NT were purchased from the Sigma–Aldrich and TCI chemicals, Japan respectively and stored in dark at room temperature before and after the spectral acquisition. THF was a good solvent for both TC and NT. On the other hand, TC and

NT were sparingly soluble in water. TC and NT colloidal aggregates were prepared by injecting a 1.0 mM solution of TC and NT in Tetrahydrofuran (THF) into a large volume of vigorously stirred ultrapure water of  $18.2 \text{ M}\Omega\cdot\text{cm}^{-1}$  resistivity under controlled volume ratios of THF to water. For steady-state optical studies, TC and NT aggregates were degassed with  $\text{N}_2$  and placed in a 1 cm path length quartz cell for absorption and emission experiments. Steady-state absorption and fluorescence experiments were performed using standard methods and instruments. The experimental UV-vis spectra of both TC and NT monomers and their aggregates were initially Gaussian fitted to accurately obtain the various electronic transitions and their associated vibronic bands. The oscillator strength for an electronic transition was experimentally calculated using:  $f = 4.32 \times 10^{-9} \int \epsilon \cdot d\bar{\nu}$ ,<sup>53</sup> where  $\int \epsilon \cdot d\bar{\nu}$ , represents area under the curve in  $\epsilon(\text{M}^{-1}\text{cm}^{-1})$  vs.  $\bar{\nu}(\text{cm}^{-1})$  plot. The frequency range [ $\bar{\nu}(\text{cm}^{-1})$ ] for oscillator strength calculation was selected on the basis of the obtained curve for the lowest energy electronic transition. The as-obtained value of oscillator strength as a theoretical quantity was converted to a more meaningful experimental quantity as the TDM ( $\vec{M}$ ), using  $\vec{M}(D) = \left(\frac{3he^2 \cdot f}{8\pi^2 m_e c \cdot \bar{\nu}}\right)^{1/2} = 0.461 \times \sqrt{f \times \lambda(\text{nm})}$ .<sup>53</sup> The magnitude of excitonic coupling energy in aggregates was calculated as  $\Delta E_{\text{exc}} = h \cdot c \left(\frac{1}{\lambda_{\text{agg}}^1} - \frac{1}{\lambda_{\text{agg}}^2}\right)$  where  $\lambda_{\text{agg}}^1$  and  $\lambda_{\text{agg}}^2$  represented absorption wavelengths for in-phase and out-of-phase arranged TDMs. The PLQY for TC and NT monomers in THF ( $n_{\text{THF}} = 1.407$ ) and TC and NT aggregates in water ( $n_w = 1.330$ ) were determined using perylene-3,4,9,10-tetracarboxylic acid (0.1 M  $\text{K}_2\text{CO}_3$ ,  $n = 1.335$ ) as a standard.<sup>54</sup>

## 2.2 HR-scanning electron microscopy

The aggregate geometry was examined by collecting high-resolution images from a field emission scanning electron microscope (Inspect F50 - FEI, USA). Sample preparation was done by drop casting aqueous suspensions of TC and NT aggregates onto a glass microscope slide and allowed to dry overnight in dark prior to use.

## 2.3 Time-correlated single photon counting experiments

Time-resolved PL decay curves were measured using the time-correlated single-photon counting technique; here, nanosecond pulsed excitations from light-emitting diodes of 296 nm and 496 nm with an instrument response function (IRF) = 260 ps were made use of with a FluoroCube, Horiba Jobin Yvon Inc. fluorescence lifetime system. Lifetime measurements for the monomers were performed on the very dilute  $1 \times 10^{-7} \text{ M}$  dye solution in THF with well-separated monomers and their negligible molecular interaction. The resulting fluorescence emission from  $\text{N}_2$  degassed samples, housed in a 1 cm path length quartz cell, was collected at right angles to the sample.

## 2.4 Nanosecond laser flash photolysis experiments

Transient absorption spectra (TAS) were recorded for NT aggregates using a nanosecond laser flash photolysis instrument (Applied Photophysics, U.K.). The transient signals were detected using a 150 W pulsed xenon lamp, a Czerny-Turner monochromator, and Hamamatsu R-928 photomultiplier tube as a detector. The pulse width of the laser light was 8 ns. The Agilent infinity digital storage oscilloscope captured the transient signals, followed by data transferring to the computer for further analysis. Colloidal aggregates suspended in a long-necked cuvette (10 mm path length) were deoxygenated by constant bubbling with argon gas for 45 min prior to the laser irradiation. Decay profiles were collected typically as the average of 4–8 shots (126 maximum) at 1–2 Hz.

## 2.5 Electronic structure calculation of TC and NT monomers and the respective dimers

The ground state optimization and electronic structure computation of monomers were performed at DFT/6-31G+(d,p)/B3LYP and TD-DFT/6-31G+(d,p)/B3LYP levels respectively following the integral equation formalism polarizable continuum model (IEFPCM) in THF using Gaussian 09 set of programs.<sup>55</sup> Even though it is cumbersome to model a complete molecular aggregate with density functional calculations, its photophysical behaviour can be well-captured *via* a dimeric model. Therefore, to obtain deeper insight on the TC O- and NT J-aggregate structures, the computed ground state and the corresponding energetics of low-lying singlet excited states in the base settings of their dimeric forms were next detailed. The equilibrium dimeric conformation of TC was unravelled by computing the globally optimized structure using the single crystal coordinates<sup>39</sup> at DFT/6-31G+(d,p)/M062X level in the water, with M062X as a hybrid meta-exchange correlation functional,<sup>56</sup> previously benchmarked<sup>45,56–58</sup> for dimers. All optimizations were performed with tight convergence criteria without any symmetry constraints, followed by frequency calculations to assure the global minimum. The TC dimeric stabilization energy was computed as the absolute energy difference between the TC dimer and double that of the TC monomer, optimized at the same theory level i.e., DFT/6-31G+(d,p)/M062X with IEFPCM in water. The initial model geometry of NT dimer was predicted based on the parallel alignment of monomeric TDMs obtained from ground state absorption studies. Subsequently, the potential energy curve was scanned at the DFT/6-31G+(d,p)/M062X level of theory by fixing  $R_1$  (intermolecular distance) constant at  $3.7 \text{ \AA}$ , typical of  $\pi$ - $\pi$  stacked dimers,<sup>59</sup> while varying the horizontal displacement  $R_2$  and noting the concomitant change in the slippage angle  $\theta$  as  $35^\circ \leq \theta \leq 90^\circ$ . The dark or bright character of the singlet excited states of TC and NT dimer were ascertained from the computed magnitudes of the oscillator strength ( $f$ ). From the methodology point of view, locally excitonic (LE) and CT states can in principle be described by standard

electronic structure methods, such as, the configuration interaction singles, TD-DFT, or equation-of-motion coupled-cluster singles and doubles. With a primary focus towards characterization of low-lying singlet excited states in this present contribution, LE or CT characteristics of the dimeric singlet excited states were unravelled following TD-DFT-M062X/6-31G+(d,p) method with IEFPCM in water. The visual inspection of LE and CT singlet states were carried out using charge density difference (CDD) plots, procured from the difference of computed electron (EDD) and hole (HDD) density distribution maps, following Multiwfn 3.3.8.<sup>60</sup> Electron ( $\rho_-(r)$ ) and hole ( $\rho_+(r)$ ) density distribution maps are characteristic regions belonging to photoexcited states. Tian Lu and Cheng Zhong have shown the EDD and HDD to be described in terms of molecular orbital wavefunction ( $\Phi$ ) and configuration coefficient ( $w$ ) corresponding to transition of an electron from occupied MO ( $i$ ) to a virtual MO ( $l$ ) upon electronic excitation,<sup>60</sup> vide equations 1 and 2.

$$\rho_-(r) = \sum_{i \rightarrow l} (w_i^l)^2 \Phi_l(r) \Phi_l(r) + \sum_{i \rightarrow l} \sum_{i \rightarrow m \neq l} w_i^l w_i^m \Phi_l(r) \Phi_m(r) \quad (1)$$

$$\rho_+(r) = \sum_{i \rightarrow l} (w_i^l)^2 \Phi_i(r) \Phi_i(r) + \sum_{i \rightarrow l} \sum_{j \neq i \rightarrow l} w_i^l w_j^l \Phi_i(r) \Phi_j(r) \quad (2)$$

The above formalism was used in the present investigation for computing EDD and HDD maps for the monomers and the dimers at TD-DFT/6-31G+(d,p) level of theory with IEFPCM in THF and water respectively. The centroids of the electron ( $C_-$ ) and hole ( $C_+$ ) density distribution, which are a qualitative and easy-to-visualize measure of the spatial extent of LE or CT were calculated following Multiwfn 3.3.8. The two centroids of charges associated with the positive ( $C_+(r)$ ) and negative ( $C_-(r)$ ) density regions were defined as:

$$C_+(r) = A_+ e \left( -\frac{(x-x_+)^2}{2\sigma_{+x}^2} - \frac{(y-y_+)^2}{2\sigma_{+y}^2} - \frac{(z-z_+)^2}{2\sigma_{+z}^2} \right) \quad (3)$$

$$C_-(r) = A_- e \left( -\frac{(x-x_-)^2}{2\sigma_{-x}^2} - \frac{(y-y_-)^2}{2\sigma_{-y}^2} - \frac{(z-z_-)^2}{2\sigma_{-z}^2} \right) \quad (4)$$

The direction of monomeric TDM was thus defined as the line passing through the centroids of EDD and HDD maps for the associated monomeric electronic transition. This approach in deducing an accurate TDM direction was previously tested by us on a p-nitroaniline monomer.<sup>45</sup> Moreover, in the optimized TC dimeric structure, the intermolecular distance 'r' along with the polarization ( $\alpha$ ) angle (an angle between monomeric TDMs) were obtained from two defined positions placed at the centres of the TC subunits and the as-computed monomeric TDM.

Obtaining a quantitative measure of the length and magnitude of CT is far from trivial both from the experimental and theoretical points of view. With an aim in defining the CT spatial extent associated with the electronic transitions, the indexes  $\varphi_{C_+C_-}$  and t, previously developed for the evaluation of excited state characteristics,<sup>61,62</sup> were estimated and detailed in Tables S6–S10, Supplementary Information. Briefly, these indexes were based on the computed electron ( $\rho_-(r)$ ) and hole ( $\rho_+(r)$ ) density distribution of the excited states. The overlap integral ( $\varphi_{C_+C_-}$ ) of  $C_-$  and  $C_+$  for the associated electronic transitions was used as a quantitative parameter for differentiating the excited states into either LE or CT state:

$$\varphi_{C_+C_-} = \int \frac{\sqrt{C_+(r)}}{A_+} \frac{\sqrt{C_-(r)}}{A_-} dr \quad (5)$$

Nonetheless, it is important to note that  $\varphi_{C_+C_-}$  is also an indicative of 'intra-molecular CT' character of the excited states. Therefore, the final assessment of the excited state character in the present context warranted a more detailed investigation. A tangible proof was obtained by evaluating the t-index in all three spatial directions using the computed EDD and HDD; a positive t-index defined the quantitative extent of intermolecular CT through space.<sup>61,62</sup> Finally, the "t" indexes representing the extent of intermolecular degree of separation between hole and the electron were calculated as:

$$t(\text{\AA}) = D_{ct}(\text{\AA}) - H(\text{\AA}) \quad (6)$$

The quantitative expressions for root mean square deviation ( $\sigma$ ) of  $C_-$  and  $C_+$  along the three axes in equations 3 and 4, normalization factors ( $A_-$  and  $A_+$ ) in equation 5,  $D_{ct}$  and H indexes in equation 6 were originally defined by Bahers *et al.*,<sup>61</sup> and in the present work were evaluated following Multiwfn 3.3.8. For  $t < 0$ , an overlap between hole and electron was expected and thus the associated electronic excited state was ascribed as LE. However, a clear separation of hole and electron on individual monomeric units led to a larger positive value of t-index, making the associated electronic excited state to be of predominant CT type. In this regard, using the total EDD and HDD computed for the singlet excited states of dimers, the evaluation of the above-mentioned indexes on a grid of points with isovalue 0.001 around the dimeric structures were established. All density derived quantities were computed using a numerical integration procedure by using Multiwfn 3.3.8. The combined use of  $\varphi_{C_+C_-}$  and t-indexes in all three spatial directions was used to ascertain the CT or LE character of the low-lying singlet excited states of TC and NT dimers.

### 3. Results and Discussion

#### 3.1 Validation of the TC O- and NT J- aggregation from steady state absorption characteristics

Solvent polarity dependent UV-vis spectroscopic signatures of TC and NT in Figure 2(a) and (b)

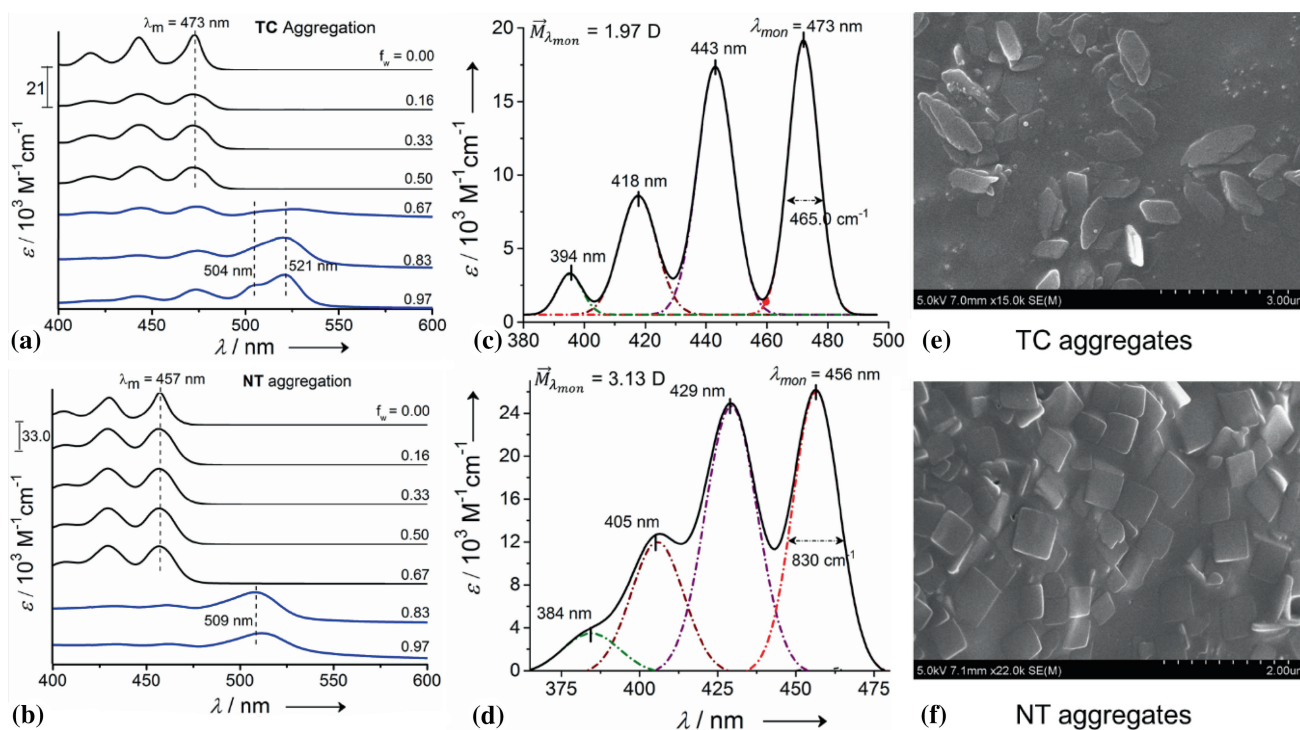


**Figure 2.** (a) and (b) Solvent polarity dependent UV-vis absorption spectra of TC and NT at a fixed concentration ( $1.67 \times 10^{-5}$  M) with the varied volume fraction of water ( $f_w$ ). The formation of self-assembled molecular aggregates of TC and NT are indicated with a red-shifted absorption band (blue curves). (c) and (d) The deconvoluted absorption spectra of TC and NT monomers respectively, depicting the associated electronic transitions and transition dipole moments ( $\vec{M}_{\lambda_{mon}}$ ). (e) and (f) The HR-SEM images of TC and NT respectively at a THF: water volume fraction of 0.1:2.9 depicting the self-assembled TC and NT aggregates.

respectively were investigated to unravel the aggregation pattern and the associated electronic processes. At  $0 \leq f_w$  (water-volume fraction)  $\leq 0.50$ , no perceptible spectroscopic change with solvent polarity was observed. However, at  $0.83 \leq f_w \leq 0.97$ , new UV-Vis absorption bands at pronounced longer wavelengths ( $\lambda_{agg} = 521$  nm for TC and  $\lambda_{agg} = 509$  nm for NT) than the monomeric absorption maximum were witnessed, indicating the formation of self-assembled TC and NT aggregates. The deconvoluted spectrum of TC monomer in Figure 2(c) depicted a predominant electronic transition at 473 nm (2.62 eV) with an oscillator strength of 0.038 ( $\vec{M}_{mon} = 1.97$  D), excellently matching with a literature value  $21,200 \text{ cm}^{-1}$  (2.63 eV).<sup>44</sup> The UV-Vis spectroscopic signatures of NT monomer in Figure 2(d) was found to be identical to TC monomer with a lowest electronic transition at  $\lambda_{mon} = 456$  nm, possessing a comparatively larger oscillator strength of 0.101 ( $\vec{M}_{mon} = 3.13$  D). The HR-SEM images in Figure 2(e) and (f) for TC and NT respectively obtained at  $f_w = 0.97$  solvent composition validated the formation of their stable colloidal aggregates with finite shape and size.

The abrupt transition from a monomeric to an aggregated phase was also evident with a concomitant visible

colour change: green to pale pink for TC (cf. Figure 3(a) inset) and bright green to yellowish brown for NT (cf. Figure 3(b) inset). The deconvoluted UV-vis absorption spectrum of TC colloidal aggregates in Figure 3(a) depicted the transition to fit Gaussians centred at 531 nm (2.34 eV) and 505 nm, in a closer match with the TC thin films.<sup>38</sup> It was interesting to note that TC aggregates exhibited significant transition probabilities for both lower ( $\lambda_{agg}^1 = 531$  nm,  $\vec{M}_{\lambda_{agg}^1} = 2.79$  D) as well as higher ( $\lambda_{agg}^2 = 505$  nm,  $\vec{M}_{\lambda_{agg}^2} = 1.59$  D) energy excitations. In contrast, the deconvoluted UV-vis spectrum of NT aggregates in Figure 3(b) depicted predominant absorption only to a lower energy exciton state [ $\lambda_{agg}^1 = 512$  nm (2.42 eV),  $\vec{M}_{\lambda_{agg}^1} = 2.69$  D] along with a meagre transition probability to a higher energy exciton state ( $\lambda_{agg}^2 = 491$  nm,  $\vec{M}_{\lambda_{agg}^2} = 0.69$  D). This uneven TDM distribution was rationalized in accordance with the theory of molecular exciton coupling.<sup>3</sup> According to this theory, a finite deviation from a parallel alignment of monomeric TDM's (relative to the ideal J- and H-dimers), as in an O-dimer (oblique dimer), should cause finite transition probabilities to both higher and lower exciton states.<sup>3</sup> In line with this, we had reported a large deviation from J- and H-aggregates for p-nitroaniline O-aggregates and

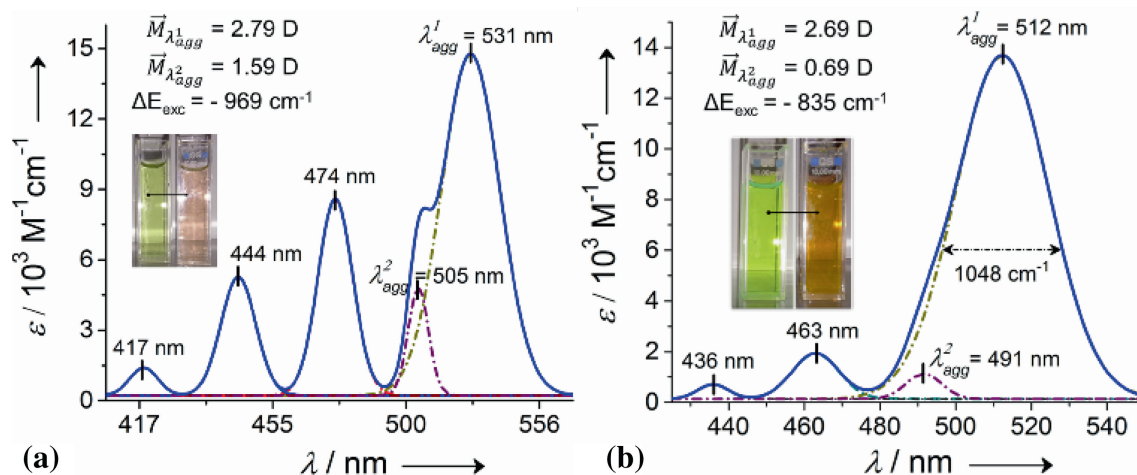


**Figure 3.** Deconvoluted UV-vis absorption spectrum of TC (a) and NT (b) aggregates ( $1.7 \times 10^{-6} \text{ M}$ ) in THF-water binary solvent depicting predominant absorption features and associated transition dipole moments along with exciton coupling energies. The insets depict the colour change upon aggregation in both TC and NT.

quantified it with the polarization angle ( $\alpha$ ), an angle subtended by the monomeric TDMs in a dimeric unit.<sup>45</sup> Therefore, based on the considerable distribution of TDMs, we assigned the TC colloidal aggregates as predominantly of O-type. In contrast, the prevalent 512 nm red-shifted absorption feature for NT was indicative of the ideal J-aggregation. It is also important to note that, the coherent coupling of monomeric TDMs resulted in similar exciton coupling energies ( $\Delta E_{exc} = -969 \text{ cm}^{-1}$  for TC O-aggregates and  $\Delta E_{exc} = -835 \text{ cm}^{-1}$  for NT J-aggregates). These large magnitudes of exciton coupling energies precluded the possibility of TC and NT excimer formation, of which more concrete evidences were captured by emission and excitation spectroscopic measurements, discussed in the following sections.

### 3.2 Unusual steady state emission characteristics of TC O- and NT J-aggregates

To obtain insights into the aggregation-induced PL characteristics, solvent polarity controlled emission signatures of TC and NT were collected in Figure 4(a) and 4(b) respectively; progressively increasing the volume fraction of water did not affect the spectra until the water fraction became 83%. The inset micro-images in Figure 4(a) and (b) depicted the TC and NT monomer solutions respectively exhibiting a bright green and cyan fluorescence under UV lamp illuminated at 365 nm. The emission spectrum (cf. Figure 4(a)) of TC monomer depicted an intense emission band at 478 nm for which the calculated PLQY was estimated to be  $\Phi_F = 0.116$

(see Figure S1, Supplementary Information). Likewise, the emission spectrum (cf. in Figure 4(b)) of the NT monomer depicted an intense emission band at 466 nm with PLQY,  $\Phi_F = 0.478$  (Figure S2, Supplementary Information). In literature, the J-type aggregation is primarily associated with a dramatic improvement in fluorescence quantum efficiency.<sup>4-6</sup> Therefore, TC O- and NT J-aggregates could be thought of supporting ‘aggregation induced enhanced emission’ phenomenon. Much to our surprise, at  $f_w = 0.97$ , emissions from the TC O- and NT J-aggregate solutions were drastically reduced in reference to the pure monomeric THF solutions (cf. micrograph in Figure 4(a) and (b) insets), indicating a virtually non-emissive behaviour of the former. The monomeric emission intensities decreased abruptly (cf. Figure 4(a) and (b)) with the onset of new, feebly intense emission bands at 535 and 524 nm respectively. Subsequently, the PLQY for the TC O-aggregates ( $\Phi_F = 0.002$ , see Figure S3, (Supplementary Information) for calculation) and NT J-aggregates ( $\Phi_F = 0.038$ , see Figure S4 (Supplementary Information) for calculation) were estimated to be dramatically lower than their corresponding monomers. Although this reduction in PLQY upon aggregation provided a clue for the possibility of a faster non-radiative deactivation channel for the  $S_1$  state or a ground state structural perturbation, the reason for such large emission quenching, especially in the J-aggregate nuclear conformation, was a huge deviation.

The large excitonic coupling energies obtained from ground state UV-Vis absorption spectra of TC O- and NT J-aggregates provided an initial indication of the absence of excimer-like species. Moreover, emission spectra obtained for TC and NT aggregates (cf.

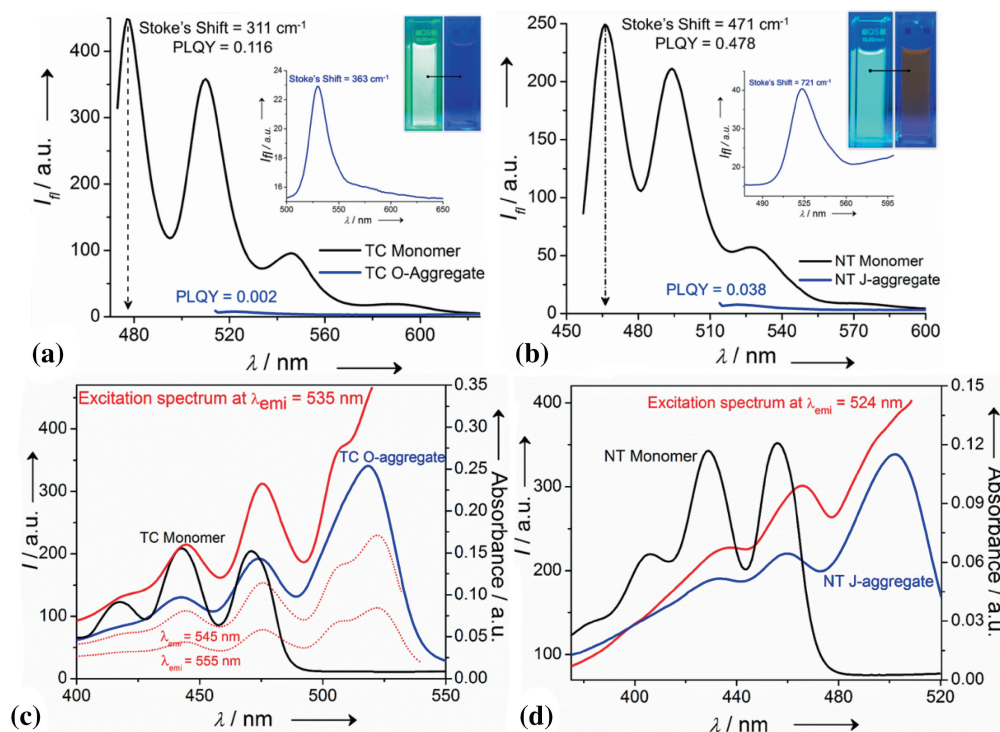


**Figure 4.** (a) and (b) Emission spectra of TC and NT monomers and the corresponding aggregates respectively, depicting fluorescence quenching with a dramatic drop in PL quantum yield (PLQY). Insets illustrate the structured, narrow band-width and low Stoke's shifted emission bands for TC O- and NT J-aggregates. The micrograph images depict the visual colour change upon aggregation under UV lamp exposure at 365 nm. (c) and (d) Excitation spectra (red) of TC O- and NT J-aggregates respectively obtained at the corresponding emission maximum depicting a close resemblance with the ground state UV-vis absorption spectrum (blue) of the aggregated form, thus ruling out the excimer formation.

Figure 4(a) and (b) insets respectively) were observed to be highly structured with extremely low Stoke's shifts and narrow bandwidths, providing additional evidence for non-excimer formation. A more concrete proof for non-excimer formation was drawn from the excitation spectral studies in Figures 4(c) and (d). Figure 4(c) depicted the collected excitation spectra of TC O-aggregates with monitoring emission wavelengths of 535, 545 and 555 nm. The spectral profile of the solution excitation spectrum was in good agreement with the corresponding TC O-aggregate solution absorption spectrum and was markedly different from the TC monomeric absorption spectrum. The sharp resemblance of excitation spectrum to that of the absorption spectrum definitely led us to the conclusion that the pronounced emission quenching observed in TC O-aggregates was not associated with the excimer formation. In Figure 4(d), similar excitation spectral results were visualized for NT J-aggregates. A close resemblance of the excitation spectrum with that of its J-aggregates absorption spectrum along with a large deviation from the NT monomeric absorption ruled out the existence of NT excimers.

In TC, photo-oxidation *via* cycloaddition studies have shown evidence for naphthalene-like spectral features.<sup>35–37</sup> Thus, in order to establish the TC O- and NT J-aggregates to be unperturbed by oxidation, their absorption and PL spectra as a function of irradiation time were recorded in the air (cf. Figures S5 (Supplementary Information) (a) and (b) respectively). In both cases, other than an overall homogeneous reduction of absorption and PL intensities, no new spectral changes have been observed. This suggests that none of the PL bands in TC O- and NT J-aggregate forms were related to naphthalene-like impurities. In contrast, a face-to-face stacked covalent TC dimer (an H-aggregate) was photo-oxidized by more than half within the first 10 min of light irradiation.<sup>37</sup> Therefore, in the present investigation SF as a process was thought of which could complicate the aggregate excited state dynamics. In order to assess the possibility of SF in TC O- and NT J-aggregates and thus to explain the consequential dramatic drops in PLQY, density functional computational calculations, time-correlated single photon counting and nanosecond transient absorption experiments were undertaken.

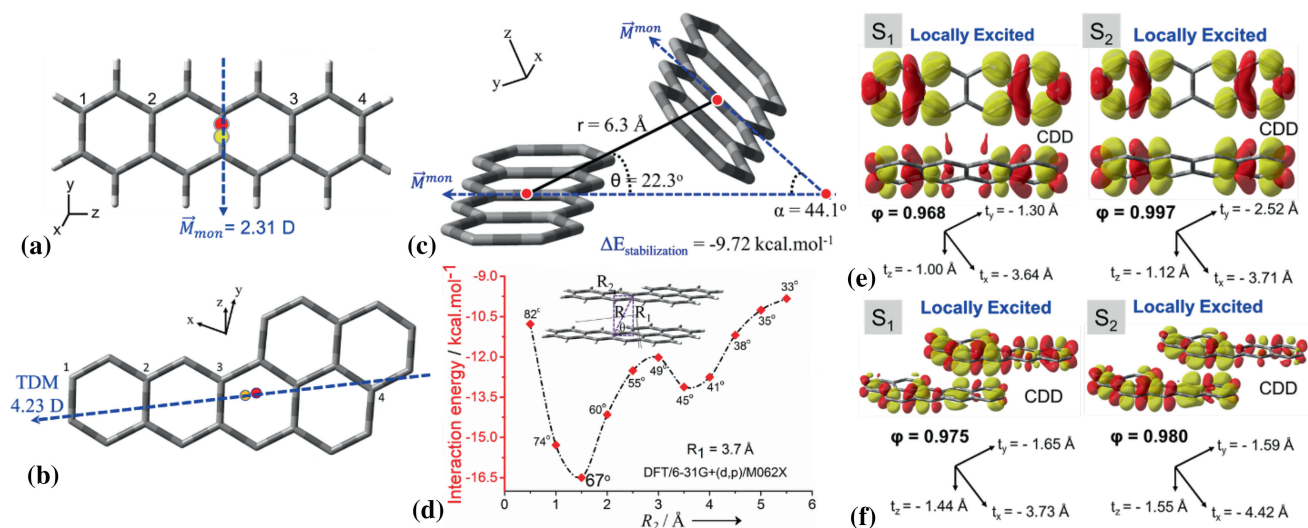


**Figure 5.** (a) and (b) The optimized structures of TC and NT monomers depicting a planar tetracene core with  $0^\circ$  dihedral angle ( $C_1-C_2-C_3-C_4$ ). The computed electronic transition dipole moment ( $\vec{M}_{mon}$ ) direction procured from electron (yellow) and hole (red) density distribution centroids are depicted with blue arrows. (c) The optimized oblique dimeric structure of TC dimer depicting the dimer stabilization energy along with slippage angle ( $\theta$ ) and a large polarization angle ( $\alpha$ ). (d) The potential energy curve for the NT dimer computed using the initial dimeric model depicted in the inset validates the stability of J-dimer at  $\theta = 45^\circ$ . (e) and (f) depict the locally excited characteristics of TC O- and NT J-dimers' bright  $S_1$  and  $S_2$  excited states. The quantitative index ( $\phi$ )  $\sim 1$  and the negative t-index signify the LE nature of both  $S_1$  and  $S_2$  excited states. Hydrogen atoms are removed for clarity.

### 3.3 TC O- and NT J-dimer excited state energetics and correlation with singlet fission

The DFT/6-31G+(d,p)/B3LYP computed ground state optimized structures of TC and NT monomers in Figure 5(a) and (b) respectively depict the planar tetracene core with a  $0^\circ$  dihedral angle ( $C_1-C_2-C_3-C_4$ ). The computed 2.43 eV electronic transition for the TC monomer involved 97% HOMO  $\rightarrow$  LUMO weighing contribution for which the computed HDD and EDD maps (Figure S6, Supplementary Information) showed a symmetrically distributed isosurface on TC core unit. The thus computed configuration coefficients for this electronic excitation along with the centroid coordinates of EDD and HDD were tabulated in Table S3, Supplementary Information, and were further used for the estimation of TDM direction. Accordingly, the computed TDM direction in Figure 5(a) was depicted as a vector passing through the shorter molecular axis of TC monomer with a magnitude of 2.31 D. In contrast to the TC monomer, the computed monomeric TDM for NT was estimated (cf. Figure S7, Supplementary Information) to be along a longer molecular axis with a higher magnitude of 4.23 D (cf. Figure 5(b)).

The ground state optimized structure of TC dimer from its single crystal coordinates<sup>39</sup> in Figure 5(c) converged to an O-dimeric conformation with  $\theta = 22.3^\circ < 54.7^\circ$  and a large  $\alpha$  ( $44.1^\circ$ ), substantiated with the monomeric TDM direction. The computed stabilization

energy for the TC dimerization was evaluated to be  $-9.72 \text{ kcal.mol}^{-1}$  ( $\Delta E_{\text{stabilization}} = (-1385.828 - 2 \times (-692.906) \text{ a.u.}) \times 627.51$ ) and was attributed to the competitive  $\pi$ - $\pi$  and C-H stacking interactions. The initial dimeric model geometry of NT, in the absence of single crystal coordinates, was based on the parallel alignment of monomeric TDMs as indicated from the ground state absorption studies. In Figure 5(d), the potential energy curve depicted two energy minima at  $\theta = 65^\circ$  and  $45^\circ$  with the former nuclear dimeric conformation being more stable. However, in view of the experimentally obtained absorption features of NT J-aggregates corresponding to  $\theta < 54.7^\circ$ , the nuclear geometry with  $\theta = 45^\circ$  was assigned to the equilibrium J-dimeric conformation of NT, and was further used for electronic structure calculation.

Electronic structure calculation on the optimized TC O-dimer showed the lowest-lying singlet excited state ( $S_1$ ) as the brightest state (oscillator strength = 0.215). The second ( $S_2$ ) singlet excited state was also bright in absorption with substantial oscillator strength (0.046). This oscillator strength distribution was in accordance with the experimentally obtained uneven TDM distribution in TC O-aggregates thus validating the level of theory adopted for dimeric computation. Likewise, the oscillator strength distribution between  $S_1$  (0.007) and  $S_2$  (0.538) in NT J-dimer complied with experimental results for NT J-aggregates.

In the next step, we assessed the LE or CT character to the bright  $S_1$  and  $S_2$  states of TC O- and NT J- dimers. For these electronic transitions, the EDD and HDD maps are presented in Figures S8–S13, Supplementary Information. The quantitative parameters ( $\sigma_-$ ,  $\sigma_+$ ,  $D_{ct}$  and  $H$  along all three spatial directions), discussed in the computational section under experimental part below, for prediction of t-indexes are tabulated in Tables S5–10, Supplementary Information. Subsequently, Figures 5(e) and (f) depict the charge density difference maps,  $\varphi_{C^+C^-}$ , t-index and the assigned LE or CT character to the bright singlet states. The  $S_1$  and  $S_2$  states could be predominantly of LE nature with a negligible amount of CT character, as visualized in the uniformly distributed CDD plots. Furthermore, the calculated overlap integrals ( $\varphi_{C^+C^-}$ ) of EDD and HDD centroids being close to unity, provided an additional evidence for their LE character. However, the negative  $t_x$ ,  $t_y$  and  $t_z$  values provided a concrete evidence for the absence of intermolecular CT character. Consequently, these low-lying  $S_1$  and  $S_2$  bright states in the TC O- and NT J-dimer were assigned LE type, analogous to the results obtained for solid TC crystals.<sup>46</sup> The calculated singlet and triplet excited state energies for investigated monomers were found underestimated by 0.15 eV in comparison to their experimental values as: for TC monomer,  $S_1 = 2.43$  vs. 2.62 eV,  $T_1 = 1.14$  vs. 1.28 eV;<sup>44</sup> for NT monomer,  $S_1 = 2.58$  vs. 2.71 eV. Accordingly, for NT monomer,  $E(T_1)$  was taken as  $\sim 1.57$  eV (1.43 eV + 0.15 eV), taking account of the correction term. However, It is worth mentioning that the absence of any noticeable emission edge within 1.37–2.06 eV (cf. Figure S14, Supplementary Information) provided an indication of  $E(T_1)$  to be  $< 1.37$  eV for the NT monomer. In the monomeric phase, the polyacene series (anthracene, tetracene, pentacene) has exhibited the lowest triplet state energies  $E(T_1)$  of 14900  $\text{cm}^{-1}$ , 10300  $\text{cm}^{-1}$  (1.28 eV) and 6300  $\text{cm}^{-1}$  respectively.<sup>44</sup> Moreover, Basu *et al.*, found both  $V_{\text{triplet}}$  (coulombic energy due to monomeric interaction) and  $D_{\text{triplet}}$  (solvatochromic shift due to dielectric changes on aggregation) for triplet excitons to be smaller than the singlet excitons by a factor of 10 or more.<sup>47</sup> Therefore, assuming the triplet energy of TC monomer to be minimally affected by aggregation, SF in its O-aggregate from  $S_1$  state seemed endothermic by  $\sim 0.22$  eV ( $\Delta E_1 = 2.34$  eV  $- 2 \times (1.28$  eV)). Supporting this, SF in crystalline TC was also reported to be endothermic (by  $\sim 500$   $\text{cm}^{-1}$ ) but still proceeded relatively rapidly in view of entropic considerations.<sup>26,27</sup> Due to this energetic ordering, triplet-triplet recombination as the reverse process of SF, to a singlet exciton could be feasible in TC O-aggregates. In NT dimer, with the experimentally investigated lowest triplet state

( $T_1$ ) energy  $< 1.37$  eV, the  $\Delta E_1$  for SF from  $S_1$  state was evaluated to be small ( $2.42 - 2 \times (1.37) = -0.32$  eV), implying the probable occurrence of SF in NT colloidal J-aggregates. It was also interesting to note that NT J-dimer failed to satisfy the primary energy criterion,  $E(S_1) \sim 2 \times (T_1)$  for triplet-triplet recombination. However, a concrete evidence for SF and triplet-triplet recombination in TC O- and NT J-aggregates in the present investigation was obtained from time-correlated single photon counting and transient absorption measurements.

### 3.4 Singlet fission in TC O- and NT J-aggregates and correlation with their unusual PL behavior

One of the first means by which SF was detected in acene crystals was through the observation of delayed fluorescence in time-resolved fluorescence measurements.<sup>25,48,49</sup> The PL decay profile for TC monomer in Figure 6(a) depicted a single exponential decay with a singlet excited state lifetime,  $\tau = 4.36$  ns, in agreement with a reported magnitude of 4.6 ns.<sup>38</sup> The time-resolved emission spectral profile for TC O-aggregates excited at 496 nm and monitored at 550 nm emission is depicted in Figure 6(a). The fluorescence spectrum remains constant over the course of the decay, indicating the decay arising from a single species. Notably, in this more polar solvent (water), the emission on the red edge of the spectrum did not decay to zero but rather to a finite baseline, indicating the presence of a longer-lived emitting species. Three exponential decays with the fastest component's lifetime ( $\tau_1 = 0.16$  ns, relative amplitude = 45.9%) even lower than the IRF (0.26 ns) was noted. A slower time constant of  $\tau_2 = 1.84$  ns (relative amplitude = 17.9%) was attributed to the decay of  $S_1$  state *via* radiative fluorescence emission. In comparison with the monomeric TC, the lifetime of the TC O-aggregate's PL decay showed obvious shortening. Earlier experimental results and theoretical analyses have proven the existence of a super-radiant exciton delocalized over 10 TC molecules with a radiative lifetime of  $12.5 \pm 2$  ns, smaller by a factor of 2.1 than that of the TC monomer.<sup>38</sup> In Figure 6(b), the emission decay profile corresponding to the TC O-aggregates was plotted on a log-scale to highlight the long-lived emission tail. In fact, this type of delayed fluorescence (DF) following an essential energetic criterion  $E(S_1) \sim 2 \times E(T_1)$  (cf. computational section) can be understood as follows:

- i. the initially created singlet excitons generate triplet excitons.<sup>50,51</sup>
- ii. the triplet excitons undergo triplet-triplet recombination following radiative decay from the singlet state.<sup>50,52</sup>

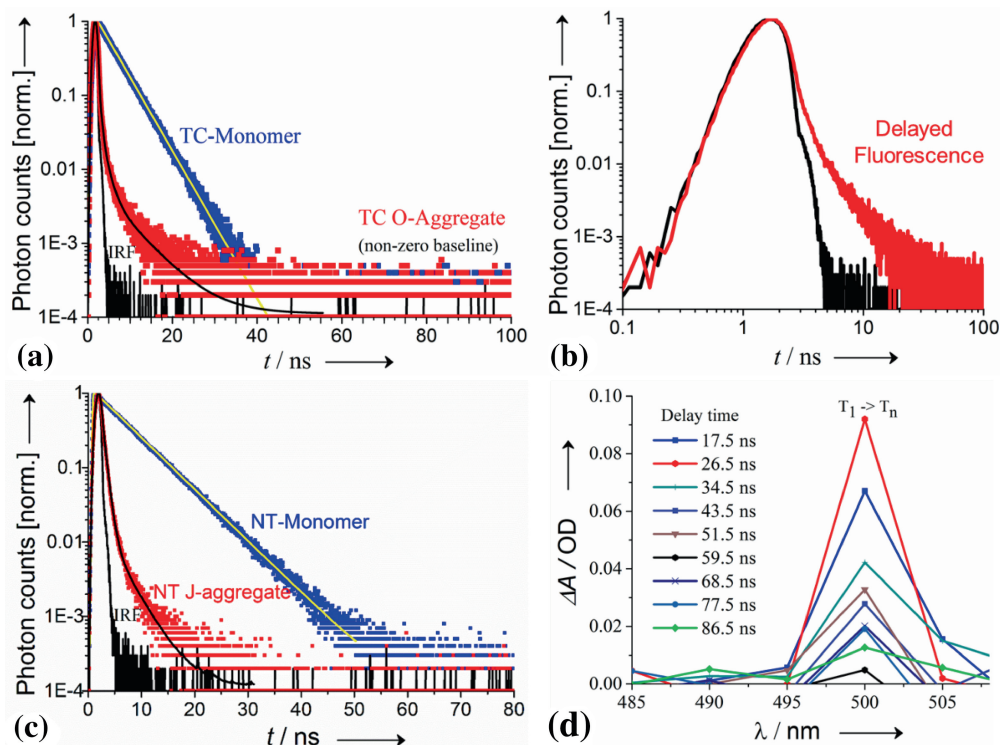


**Figure 6.** (a) Time correlated PL decay profiles (with their fits) for TC monomer (blue dotted) and TC O-aggregate (red dotted) acquired at 496 nm excitation, depicting a short and a long lifetime component in the aggregate. (b) The decay profile for TC O-aggregate observed in (a) plotted on a log-scale to highlight the long-lived emission tail. (c) PL decay profiles at varied emission wavelengths for NT J-aggregates acquired at 295 nm excitation, depicting the absence of delayed fluorescence at the lower emission wavelength (320 nm). (d) Nanosecond transient absorption spectra for the NT colloidal J-aggregates at different delay times depicting long-lived triplet absorption.

Accordingly, in Figure 6(a) and (b), the slowest third decay component ( $\tau_3 = 9.71$  ns, relative amplitude 36.2%) in TC O-aggregates was ascribed to DF occurring *via* SF and followed by triplet-triplet recombination. This phenomenon has been previously observed in TC single crystals where the lifetime of the triplet state was measured as high as 200  $\mu$ s.<sup>31,32</sup> In contrast, in TC polycrystalline samples, the lifetime was evidently smaller (40–100  $\mu$ s) and was attributed to the presence of defect states accelerating SF.<sup>30–32</sup> Hence, we assigned TC O-aggregates to undergo SF from the singlet excited state leading to fluorescence quenching, a rare case for TC O-aggregates in solution.

In Figure 6(c), the time-resolved PL decay profiles for NT monomers and the corresponding J-aggregates are depicted. The NT monomer, like its homologue TC monomer, exhibited a single exponential decay with a lifetime of 6.24 ns (cf. Figure 6(c)). However, the PL decay profile for the NT J-aggregates collected at 496 nm excitation (with a monitoring emission wavelength of 530 nm) was largely different from the TC O-aggregates with meagre longer-lived emission

signatures ( $\tau_3 = 24.1$  ns, relative amplitude = 5%). Nevertheless, the absence of highly intense long-lived emission signature or DF need not comply with the non-occurrence of SF. The major PL decay component for the NT J-aggregates with a relative amplitude of 71.0% was evident to decay at a time scale of  $\tau_1 = 0.22$  ns, lower than the IRF = 0.26 ns. A minor PL component was demonstrated to decay within  $\tau_2 = 0.80$  ns (relative amplitude = 24%), attributed to the faster radiative relaxation channel for NT J-aggregates relative to the NT monomer. Subsequently, triplet formation *via* SF in NT J-aggregates was assessed using Flash Photolysis experiments. In Figure 6(d), the transient absorption spectra of NT J-aggregates measured under 530 nm excitation led to a positive absorption band at  $\sim 500$  nm. The NT J-aggregates thus exhibited the  $S_1$  deactivation *via* SF, analogous to the TC O-aggregates. The limited 8 ns timing resolution of the transient absorption experiments restricted capturing the triplet state for the TC O-aggregate.

In Figure 7, we have provided a schematic representation of TC O- and NT J-dimeric structure-property

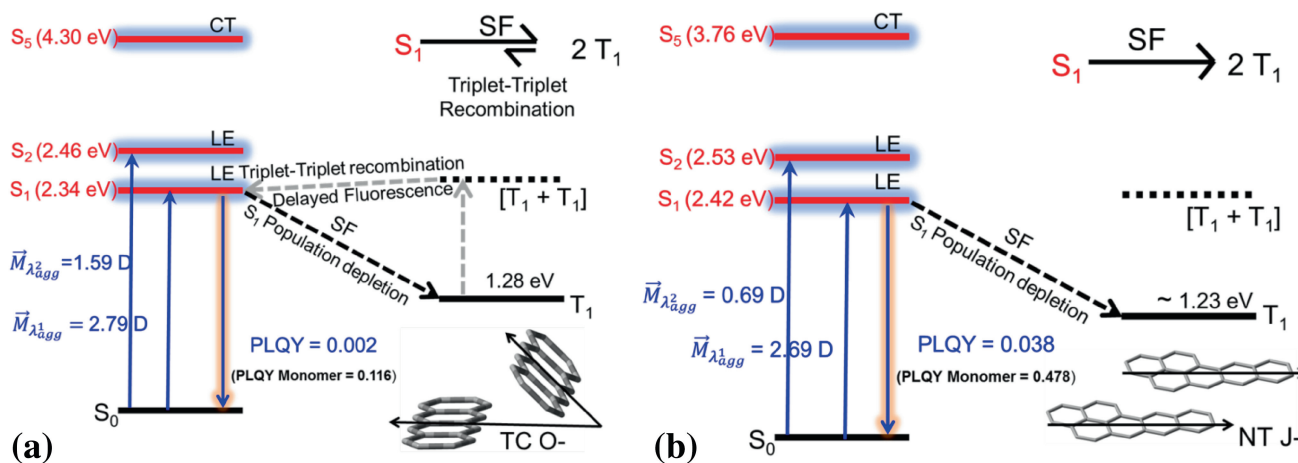


**Figure 7.** The bright singlet states of TC O- in (a) and NT J-aggregates in (b) with their experimentally obtained energies, electronic transition dipole moments and locally excited (LE) vs. charge transfer character (CT) states are depicted. The dominant  $S_1$  relaxation *via* singlet fission (SF) are correlated with the concomitant photoluminescence quantum yield (PLQY) drops.

correlation with a strong emphasis on their photoluminescence behaviour. Figures 7(a) and (b) depict the thermodynamic feasibility of SF from a bright locally excited  $S_1$  state leading to a fast  $S_1$  population depletion with a concomitant long-lived triplet formation. During such a time span, the triplets in TC O-aggregates diffused throughout the aggregate experiencing triplet-triplet recombination, thus producing emissive singlet excitons. Here, the favourable  $S_1$  and  $T_1$  energy disposition allowed triplet-triplet recombination, as witnessed *via* delayed fluorescence signals.

To summarize, our previously reported RB J-aggregates<sup>11</sup> were ‘weakly’ coupled and exhibited a significantly low magnitude of exciton coupling energy ( $\Delta E_{\text{exc}} = -358\text{cm}^{-1}$ ) owing to weak electronic communication between its largely separated subunits ( $r = 7.2 \text{ \AA}$ ) and a restricted exciton delocalization on its J-dimer, that led to an atypical PLQY drop. In comparison to this, the NT J-aggregates with polarization angle  $\alpha \sim 0^\circ$  and TC O-aggregates with  $\alpha = 44.1^\circ$  were ‘strongly’ exciton coupled ( $\Delta E_{\text{exc}} = -835\text{cm}^{-1}$  and  $-969 \text{ cm}^{-1}$  respectively) and exhibited unusual PLQY drops. Pensack *et al.*,<sup>63</sup> reported weakly coupled chromophores of Pentacene derivatives to exhibit a non-exponential triplet formation kinetics, while the strongly coupled chromophores displayed triplet formation kinetics associated with intrinsic SF rates. Thus, it is apparent that weak excitonic interactions correlate with significantly slower rates of SF, whereas strong excitonic interactions promote rapid SF. Recently, two polymorphs (A and B) of 1,3-diphenylisobenzofuran with similar dimeric conformation, but with largely varying  $\Delta E_{\text{exc}}$  of  $\sim 1900 \text{ cm}^{-1}$  (A) and  $280 \text{ cm}^{-1}$  (B) revealed a direct correlation with their SF efficiency of

200% and  $< 5\%$  respectively.<sup>64</sup> Likewise, the ultrafast SF time constant of 530 fs in polycrystalline Hexacene films was attributed to a pronounced  $\Delta E_{\text{exc}} \sim 2500 \text{ cm}^{-1}$ .<sup>65</sup> Since single-electron excitation in the SF based systems evolved to be bimolecular,<sup>66</sup> the weakly coupled RB J-aggregates represented an ideal case for SF consequential PL origin. In the present investigation, all dimers, TC, NT and RB, showed perfect energy balance between the computed singlet and triplet exciton energies for SF. The dominant  $S_1$  relaxation pathways and dynamics of TC O-, NT J- and RB J- aggregates being largely dominated by SF decay, depicted a pronounced depleted population leading to dramatic lowering in PLQY that followed high thermodynamic probability for SF. These results have thus accounted for the pronounced deviation from the well-established aggregation induced enhanced emission observed in classical dye J-aggregates.

#### 4. Conclusions

Tetracene (TC) and Naphtho[2,1,8-*qra*]tetracene (NT) as prototypical molecular materials of polyacenes formed colloidal O- and J-aggregates respectively *via* reprecipitation method. The O- and J-type molecular aggregation was evident from the uneven electronic transition dipole moment distributions to the lower and the higher energy singlet excited states. The excited state characters of the lower ( $S_1$  and  $S_2$ ) singlet excited states were carefully assessed and found to be of locally excited in nature. Unusual drops in the photoluminescence quantum yield in TC O- and NT J-aggregates were witnessed. These dramatic PL drops were systematically

investigated for the possible occurrence of excimer-like emission quenching and/or photo-degradation of the Tetracene core unit and were proven absent. In view of the TC O-aggregates exhibiting a perfect energetic balance for SF and a concomitant delayed fluorescence signal, their PL decay characteristics was ultimately attributed to the SF followed by triplet-triplet recombination. In contrast, NT J-aggregates permitted only a forward SF process, leading to a long-lived triplet formation. Consequently, the singlet excited state ( $S_1$ ) dynamics of both TC O- and NT J-aggregates was largely governed by the fast SF decay channel, resulting in a depleted singlet excited state population and therefore accounted for the atypical deviation from the well-established aggregation induced enhanced emission from classical dye J-aggregates.

### Supplementary Information (SI)

Tables S1–S10 and Figures S1–S16 are available at [www.ias.ac.in/chemsci](http://www.ias.ac.in/chemsci).

### Acknowledgements

N. A. thanks CSIR, New Delhi, for a Research Fellowship. P. G. Senapathy centre for computing resources, Sophisticated Analytical Instrumental Facility (SAIF) and Department of Chemical Engineering, IIT-Madras, are gratefully acknowledged for providing excellent Computing, TCSPC and HRSEM facilities. Grateful thanks are due to Dr. Soumya, Laser Flash Photolysis Laboratory at IIT-Madras for carrying out the nanosecond Flash Photolysis experiments. The authors thank CSIR, New Delhi, India, Grant no. 01(2830)/15/EMR-II for financial support.

### References

- Scholes G D and Rumbles G 2006 Excitons in nanoscale systems *Nat. Mater.* **5** 683
- Würthner F, Kaiser T E and Saha-Möller C R 2011 J-aggregates: From serendipitous discovery to supramolecular engineering of functional dye materials *Angew. Chem. Int. Ed.* **50** 3376
- Kasha M, Rawls H and El-Bayoumi M A 1965 The exciton model in molecular spectroscopy *Pure Appl. Chem.* **11** 371
- Kasha M, Rawls H and El-Bayoumi M A 1965 The exciton model in molecular spectroscopy *Pure Appl. Chem.* **11** 371
- An B-K, Kwon S-K, Jung S-D and Park S Y 2002 Enhanced emission and its switching in fluorescent organic nanoparticles *J. Am. Chem. Soc.* **124** 14410
- Kar H and Ghosh S 2016 J-aggregation of a sulfur-substituted naphthalenediimide (NDI) with remarkably bright fluorescence *Chem. Commun.* **52** 8818
- Basak S, Nandi N, Bhattacharyya K, Datta A and Banerjee A 2015 Fluorescence from an H-aggregated naphthalenediimide based peptide: Photophysical and computational investigation of this rare phenomenon *Phys. Chem. Chem. Phys.* **17** 30398
- Rösch U, Yao S, Wortmann R and Würthner F 2006 Fluorescent H-aggregates of merocyanine dyes *Angew. Chem. Int. Ed.* **45** 7026
- Bayda M, Dumoulin F, Hug G L, Koput J, Gorniak R and Wojcik A 2017 Fluorescent H-aggregates of an asymmetrically substituted mono-amino Zn(II) phthalocyanine *Dalton Trans.* **46** 1914
- Miguel G de, Ziolkowski M, Zitnan M, Organero J A, Pandey S S, Hayase S and Douha A 2012 Photophysics of H- and J-aggregates of indole-based squaraines in solid state *J. Phys. Chem. C* **116** 9379
- Aggarwal N and Patnaik A 2017 Unusual non-emissive behavior of rubrene J-aggregates: A rare violation *J. Phys. Chem. B* **121** 3190
- Jelley E E 1936 Spectral absorption and fluorescence of dyes in the molecular state *Nature* **138** 1009
- Lee J, Jadhav P, Reuswig P D, Yost S R, Thompson N J, Congreve D N, Hontz E, Van Voorhis T and Baldo M A 2013 Singlet exciton fission photovoltaics *Acc. Chem. Res.* **46** 1300
- Jadhav P J, Mohanty A, Sussman J, Lee J and Baldo M A 2011 Singlet exciton fission in nanostructured organic solar cells *Nano Lett.* **11** 1495
- Ehrler B, Wilson M W B, Rao A, Friend R H and Greenham N C 2012 Singlet exciton fission-sensitized infrared quantum dot solar cells *Nano Lett.* **12** 1053
- Rao A, Wilson M W B, Hodgkiss J M, Albert-Seifried S, Bäessler H and Friend R H 2010 Exciton fission and charge generation via triplet excitons in pentacene/C60 bilayers *J. Am. Chem. Soc.* **132** 12698
- Congreve D N, Lee J, Thompson N J, Hontz E, Yost S R, Reuswig P D, Bahlke M E, Reineke S, Van Voorhis T and Baldo M A 2013 External quantum efficiency above 100% in a singlet-exciton-fission-based organic photovoltaic cell *Science* **340** 334
- Picciolo L C, Murata H and Kafafi Z H 2001 Organic light-emitting devices with saturated red emission using 6,13-diphenylpentacene *Appl. Phys. Lett.* **78** 2378
- Wolak M A, Jang B-B, Palilis L C and Kafafi Z H 2004 Functionalized pentacene derivatives for use as red emitters in organic light-emitting diodes *J. Phys. Chem. B* **108** 5492
- Xu Q, Duong H M, Wudl F and Yang Y 2004 Efficient single-layer “twistacene”-doped polymer white light-emitting diodes *Appl. Phys. Lett.* **85** 3357
- Merlo J A, Newman C R, Gerlach C P, Kelley T W, Muires D V, Fritz S E, Toney M F and Frisbie C D 2005 p-Channel organic semiconductors based on hybrid acenethiophene molecules for thin-film transistor applications *J. Am. Chem. Soc.* **127** 3997
- Tang M L, Reichardt A D, Miyaki N, Stoltenberg R M and Bao Z 2008 Ambipolar, high performance, acene-based organic thin film transistors *J. Am. Chem. Soc.* **130** 6064
- Smith M B and Michl J 2013 Recent advances in singlet fission *Annu. Rev. Phys. Chem.* **64** 361
- Ma L, Zhang K, Kloc C, Sun H, Michel-Beyerle M E and Gurzadyan G G 2012 Singlet fission in rubrene single crystal: direct observation by femtosecond

- pump–probe spectroscopy *Phys. Chem. Chem. Phys.* **14** 8307
25. Singh S, Jones W J, Siebrand W, Stoicheff B P and Schneider W G 1965 Laser generation of excitons and fluorescence in anthracene crystals *J. Chem. Phys.* **42** 330
26. Chan W-L, Ligges M and Zhu X Y 2012 The energy barrier in singlet fission can be overcome through coherent coupling and entropic gain *Nat. Chem.* **4** 840
27. Wilson M W B, Rao A, Johnson K, Gélinas S, di Pietro R, Clark J and Friend R H 2013 Temperature-independent singlet exciton fission in tetracene *J. Am. Chem. Soc.* **135** 16680
28. Birech Z, Schwoerer M, Schmeiler T, Pflaum J and Schwoerer H 2014 Ultrafast dynamics of excitons in tetracene single crystals *J. Chem. Phys.* **140** 114501
29. Arnold S and Whitten W B 1981 Temperature dependence of the triplet exciton yield in fission and fusion in tetracene *J. Chem. Phys.* **75** 1166
30. Burdett J J and Bardeen C J 2013 The dynamics of singlet fission in crystalline tetracene and covalent analogs *Acc. Chem. Res.* **46** 1312
31. Grumstrup E M, Johnson J C and Damrauer N H 2010 Enhanced triplet formation in polycrystalline tetracene films by femtosecond optical-pulse shaping *Phys. Rev. Lett.* **105** 257403
32. Tayebjee M J Y, Clady R G C R and Schmidt T W 2013 The exciton dynamics in tetracene thin films *Phys. Chem. Chem. Phys.* **15** 14797
33. Swenberg C E and Stacy W T 1968 Bimolecular radiationless transitions in crystalline tetracene *Chem. Phys. Lett.* **2** 327
34. Peter G and Bässler H 1980 Fluorescence and energy transfer in disordered solid tetracene *Chem. Phys.* **49** 9
35. Reichwagen J, Hopf H, Del Guerzo A, Desvergne J-P and Bouas-Laurent H 2004 Photodimers of a soluble tetracene derivative. Excimer fluorescence from the head-to-head isomer *Org. Lett.* **6** 1899
36. Iannone M A and Scott G W 1990 Low temperature emission spectra of trapped tetracene pairs from ditetracene *Chem. Phys. Lett.* **171** 569
37. Liu H, Nichols V M, Shen L, Jahansouz S, Chen Y, Hanson K M, Bardeen C J and Li X 2015 Synthesis and photophysical properties of a “face-to-face” stacked tetracene dimer *Phys. Chem. Chem. Phys.* **17** 6523
38. Lim S-H, Bjorklund T G, Spano F C and Bardeen C J 2004 Exciton delocalization and superradiance in tetracene thin films and nanoaggregates *Phys. Rev. Lett.* **92** 107402
39. Robertson J M, Sinclair V C and Trotter J 1961 The crystal and molecular structure of tetracene *Acta Cryst.* **14** 697
40. Beljonne D, Yamagata H, Brédas J L, Spano F C and Olivier Y 2013 Charge-transfer excitations steer the Davydov splitting and mediate singlet exciton fission in pentacene *Phys. Rev. Lett.* **110** 226402
41. Greyson E C, Vura-Weis J, Michl J and Ratner M A 2010 Maximizing singlet fission in organic dimers: Theoretical investigation of triplet yield in the regime of localized excitation and fast coherent electron transfer *J. Phys. Chem. B* **114** 14168
42. Greyson E C, Stepp B R, Chen X, Schwerin A F, Paci I, Smith M B, Akdag A, Johnson J C, Nozik A J, Michl J and Ratner M A 2010 Singlet Exciton Fission for Solar Cell Applications: Energy Aspects of Interchromophore Coupling *J. Phys. Chem. B* **114** 14223
43. Hestand N J and Spano F C 2017 Molecular aggregate photophysics beyond the Kasha model: Novel design principles for organic materials *Acc. Chem. Res.* **50** 341
44. Murov S L, Carmichael I and Hug G L 1993 In *Handbook of Photochemistry* (New York: Marcel Dekker)
45. Aggarwal N and Patnaik A 2015 A new class of nitroanilinic dimer, the PNA O-dimer: Electronic structure and emission characteristics of O-dimeric aggregates *J. Phys. Chem. A* **119** 8388
46. Yamagata H, Norton J, Hontz E, Olivier Y, Beljonne D, Brédas J L, Silbey R J and Spano F C 2011 The nature of singlet excitons in oligoacene molecular crystals *J. Chem. Phys.* **134** 204703
47. Basu S 1964 In *Advances in Quantum Chemistry* Vol. 1 Per-Olov Löwdin (Ed.) (New York and London: Academic Press) p. 145
48. Groff R P, Avakian P and Merrifield R E 1970 Coexistence of exciton fission and fusion in tetracene crystals *Phys. Rev. B* **1** 815
49. Johnson R C and Merrifield R E 1970 Effects of magnetic fields on the mutual annihilation of triplet excitons in anthracene crystals *Phys. Rev. B* **1** 896
50. Kepler R G, Caris J C, Avakian P and Abramson E 1963 Triplet excitons and delayed fluorescence in anthracene crystals *Phys. Rev. Lett.* **10** 400
51. Ern V, Avakian P and Merrifield R E 1966 Diffusion of triplet excitons in anthracene crystals *Phys. Rev.* **148** 862
52. Hall J L, Jennings D A and McClintock R M 1963 Study of anthracene fluorescence excited by the ruby giant-pulse laser *Phys. Rev. Lett.* **11** 364
53. Hilborn R C 1982 Einstein coefficients, cross sections, f values, dipole moments, and all that *Am. J. Phys.* **50** 982
54. Langhals H, Karolin J and Johansson L B-Å 1998 Spectroscopic properties of new and convenient standards for measuring fluorescence quantum yields *J. Chem. Soc. Faraday Trans.* **94** 2919
55. Frisch M J, Trucks G W, Schlegel H B, Scuseria G E, Robb M A, Cheeseman J R, Scalmani G, Barone V, Mennucci B, Petersson G A, Nakatsuji H, Caricato M, Li X, Hratchian H P, Izmaylov A F, Bloino J, Zheng G, Sonnenberg J L, Hada M, Ehara M, Toyota K, Fukuda R, Hasegawa J, Ishida M, Nakajima T, Honda Y, Kitao O, Nakai H, Vreven T, Montgomery Jr. J A, Peralta J E, Ogliaro F, Bearpark M J, Heyd J, Brothers E N, Kudin K N, Staroverov V N, Kobayashi R, Normand J, Raghavachari K, Rendell A P, Burant J C, Iyengar S S, Tomasi J, Cossi M, Rega N, Millam N J, Klene M, Knox J E, Cross J B, Bakken V, Adamo C, Jaramillo J, Gomperts R, Stratmann R E, Yazyev O, Austin A J, Cammi R, Pomelli C, Ochterski J W, Martin R L, Morokuma K, Zakrzewski V G, Voth G A, Salvador P, Dannenberg J J, Dapprich S, Daniels A D, Farkas Ö, Foresman J B, Ortiz J V, Cioslowski J and Fox D J Gaussian, Inc.: Wallingford CT USA 2009

56. Zhao Y and Truhlar D G 2007 The M06 suite of density functionals for main group thermochemistry, thermochemical kinetics, noncovalent interactions, excited states, and transition elements: two new functionals and systematic testing of four M06-class functionals and 12 other functionals *Theor. Chem. Acc.* **120** 215
57. Sutton C, Sears J S, Coropceanu V and Brédas J-L 2013 Understanding the density functional dependence of DFT-calculated electronic couplings in organic semiconductors *J. Phys. Chem. Lett.* **4** 919
58. Li R, Zheng J and Truhlar D G 2010 Density functional approximations for charge transfer excitations with intermediate spatial overlap *Phys. Chem. Chem. Phys.* **12** 12697
59. Sinnokrot M O, Valeev E F and Sherrill C D 2002 Estimates of the ab initio limit for  $\pi - \pi$  interactions: The benzene dimer *J. Am. Chem. Soc.* **124** 10887
60. Lu T and Chen F 2012 Multiwfn: A multifunctional wavefunction analyzer *J. Comput. Chem.* **33** 580
61. Le Bahers T, Adamo C and Ciofini I 2011 A qualitative index of spatial extent in charge-transfer excitations *J. Chem. Theory Comput.* **7** 2498
62. Ciofini I, Le Bahers T, Adamo C, Odobel F and Jacquemin D 2012 Through-space charge transfer in rod-like molecules: Lessons from theory *J. Phys. Chem. C* **116** 11946
63. Pensack R D, Tilley A J, Parkin S R, Lee T S, Payne M M, Gao D, Jahnke A A, Oblinsky D G, Li P-F, Anthony J E, Seferos D S and Scholes G D 2015 Exciton delocalization drives rapid singlet fission in nanoparticles of acene derivatives *J. Am. Chem. Soc.* **137** 6790
64. Johnson J C, Nozik A J and Michl J 2013 The role of chromophore coupling in singlet fission *Acc. Chem. Res.* **46** 1290
65. Busby E, Berkelbach T C, Kumar B, Chernikov A, Zhong Y, Hlaing H, Zhu X Y, Heinz T F, Hybertsen M S, Sfeir M Y, Reichman D R, Nuckolls C and Yaffe O 2014 Multiphonon relaxation slows singlet fission in crystalline hexacene *J. Am. Chem. Soc.* **136** 10654
66. Smith M B and Michl J 2010 Singlet fission *Chem. Rev.* **110** 6891